nanomaterials

MDPI

Article

Properties of S-Functionalized Nitrogen-Based MXene (Ti_2NS_2) as a Hosting Material for Lithium-Sulfur Batteries

Chenghao Yao [1,2], Wei Li [1,2,3,4,*], Kang Duan [1,2], Chen Zhu [1,2], Jinze Li [1,2], Qingyin Ren [1,2] and Gang Bai [1,2]

[1] College of Electronic and Optical Engineering and College of Microelectronics, Jiangsu Optical Communication Engineering Technology Research Center, Nanjing University of Posts and Telecommunications, Nanjing 210023, China; 1219023526@njupt.edu.cn (C.Y.); 1219023527@njupt.edu.cn (K.D.); Zhuchen@njupt.edu.cn (C.Z.); LiJinze@njupt.edu.cn (J.L.); Rqy@njupt.edu.cn (Q.R.); Baigang@njupt.edu.cn (G.B.)
[2] Jiangsu Province Engineering Research Center for Fabrication and Application of Special Optical Fiber Materials and Devices, Nanjing 210093, China
[3] State Key Laboratory of Luminescent Materials and Devices, South China University of Technology, Guangzhou 510641, China
[4] State Key Laboratory of Bioelectronics, Southeast University, Nanjing 210096, China
* Correspondence: liw@njupt.edu.cn

Abstract: Lithium-sulfur (Li-S) batteries have received extensive attention due to their high theoretical specific capacity and theoretical energy density. However, their commercialization is hindered by the shuttle effect caused by the dissolution of lithium polysulfide. To solve this problem, a method is proposed to improve the performance of Li-S batteries using Ti_2N(Ti_2NS_2) with S-functional groups as the sulfur cathode host material. The calculation results show that due to the mutual attraction between Li and S atoms, Ti_2NS_2 has the moderate adsorption energies for Li_2S_x species, which is more advantageous than Ti_2NO_2 and can effectively inhibit the shuttle effect. Therefore, Ti_2NS_2 is a potential cathode host material, which is helpful to improve the performance of Li-S batteries. This work provides a reference for the design of high-performance sulfur cathode materials.

Keywords: Li-S batteries; first-principles study; S-functionalized Ti_2N

Citation: Yao, C.; Li, W.; Duan, K.; Zhu, C.; Li, J.; Ren, Q.; Bai, G. Properties of S-Functionalized Nitrogen-Based MXene (Ti_2NS_2) as a Hosting Material for Lithium-Sulfur Batteries. *Nanomaterials* **2021**, *11*, 2478. https://doi.org/10.3390/nano11102478

Academic Editors: Xianfu Wang and Jung Woo Lee

Received: 24 August 2021
Accepted: 16 September 2021
Published: 23 September 2021

1. Introduction

Presently, the continuous development of electric vehicles and electronic devices puts more requirements on rechargeable batteries [1]. At present, the technology of lithium batteries is relatively mature, but the low theoretical capacity of them cannot meet the needs of future development [2]. Therefore, new rechargeable battery technologies need to be developed. In the next generation of rechargeable batteries, Li-S batteries have received widespread attention because of their high theoretical specific capacity and high energy density. The charge and discharge of Li-S batteries are based on a chemical reaction: $S_8 + 8Li_2 \leftrightarrow 8Li_2S$. During discharging process, the lithium anode is oxidized to form lithium ions and electrons. The lithium ions and electrons travel to the cathode via a membrane and an external circuit, respectively. Sulfur is reduced at the cathode and reacts with lithium ions and electrons to first form soluble intermediates Li_2S_8, Li_2S_6, Li_2S_4, and then form insoluble Li_2S_2 and Li_2S (Figure 1). The charging process is reversed [3,4]. The theoretical specific capacity of Li-S batteries can reach 1675 $mAh \cdot g^{-1}$, and the theoretical energy density can reach 2600 $Wh \cdot kg^{-1}$ [5–7]. In addition, as a cathode material, the sulfur has the advantages of large storage capacity, low cost, environmental friendliness, and non-toxicity [8–10]. However, in the process of charging and discharging, the long-chain soluble polysulfides (Li_2S_8, Li_2S_6, Li_2S_4) produced at the cathode of Li-S batteries are easily dissolved in the electrolyte. These soluble lithium polysulfides (LiPSs) can shuttle with the electrolyte to the anode ("shuttle effect"), causing the loss of cathode active materials. As a result, the coulombic efficiency of the Li-S batteries is reduced, and the cycle stability is

deteriorated [11–13]. In addition, sulfur and its discharge products Li_2S/Li_2S_2 have poor conductivity [14]. The application of Li-S batteries is hindered by these problems.

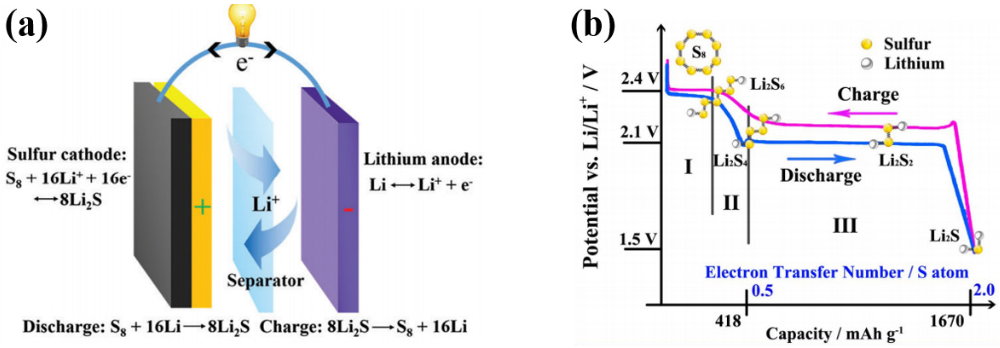

Figure 1. (**a**) Schematic of the electrochemistry, reprinted from [3]. Copyright 2016 with permission from Royal Society of Chemistry. (**b**) Charge-discharge profiles of Li-S batteries, reprinted from [4]. Copyright 2016 with permission from Elsevier.

To solve the above-mentioned problems, a lot of efforts have been made. Physical confinement is one of the effective methods [15]. Various structures, such as the open porous structure [16] and the lithium permeable shell [17], have been shown to inhibit the shuttle effect. In 2009, Nazar et al. [18] used CMK-3, a mesoporous carbon, as a conductive skeleton loaded with elemental sulfur, greatly improving the performance of the cathode. In 2018, Ma [19] et al. used the hollow carbon sphere structure as the main body of the sulfur cathode, which effectively improved the stability of the lithium–sulfur batteries.

Another effective method is chemical binding, which uses host materials with high conductivity and appropriate affinity to capture LiPSs [20]. Therefore, a variety of materials have been introduced into sulfur cathodes as host materials, such as graphene [21–23], two-dimensional transition metal sulfides and oxides [24–26], phosphorene [27–29], etc., which have been proved to be possible as cathode host materials.

Recently, *MXenes*, a new type of two-dimensional materials, have received extensive attention due to their high specific surface area, good electrical conductivity and stable structure [30–32]. It is considered to have great potential to become excellent sulfur cathode host materials. In 2015, Xiao Liang et al. [33] introduced Ti_2C into the cathode of Li-S batteries and produced the 70 wt.% S/Ti_2C composite materials, which proved that there was a strong interaction between LiPSs and Ti atoms on the surface of Ti_2C. This allowed the specific capacity of the sulfur cathodes to reach 1200 $mAh{\cdot}g^{-1}$, therefore improving the cycle performance of the sulfur cathodes. The sulfur cathodes still had a capacity retention rate of 80% after 400 cycles of charging and discharging at a rate of 0.5 C. In 2018, Chang Du et al. [34] used Ti_2O hollow nanospheres to wrap sulfur, which was then embedded in the Ti_2C interlayer to produce the $S@Ti_2O/Ti_2C$ composite materials as the cathodes of Li-S batteries. When the $S@Ti_2O/Ti_2C$ composite cathode was charged and discharged at a rate of 0.2 C, its initial capacitance reached 1408.6 $mAh{\cdot}g^{-1}$. Under the conditions of 2 C and 5 C high-rate charging and discharging after 200 cycles, it could maintain the specific capacities of 464.0 $mAh{\cdot}g^{-1}$ and 227.3 $mAh{\cdot}g^{-1}$, respectively.

As *MXenes* are etched with HF acid, functional groups are inevitably left on the surface of *MXenes* [35]. Common natural functional groups are –O, –F, –OH [36]. The presence of functional groups affects the anchoring effects of *MXenes* on LiPSs. In 2019, Dashuai Wang et al. [37] studied the anchoring effects of Ti_3C_2 surface functional groups on LiPSs through first-principles calculations. The results showed that the anchoring effects of O-functionalized Ti_3C_2 ($Ti_3C_2O_2$) on LiPSs were better than those of F-functionalized Ti_3C_2 ($Ti_3C_2F_2$). Recently, some studies have shown that it is possible to introduce non-natural functional groups, such as S-functional groups, through experimental means. Unlike natural functional groups, there are few studies on non-natural functional groups. In this work, through first-principles calculations, the adsorption capacity, electronic properties

and catalytic capacity of S-functionalized Ti_2N (Ti_2NS_2) for LiPSs are studied. The research results show that Ti_2NS_2 has a moderate adsorption capacity for LiPSs, which is stronger than O-functionalized Ti_2N (Ti_2NO_2). In addition, Ti_2NS_2 has good electrical conductivity, and it still has good electrical conductivity after adsorption of Li_2S_x species. Therefore, Ti_2NS_2 has the potential to become host materials for the cathodes of Li-S batteries.

2. Method and Computational Details

In this work, all first-principles calculations are based on the CASTEP package. The exchange-correlation functional is described by the Perdew-Burke-Ernzerhof (PBE) functional within generalized gradient approximation (GGA) [38]. The Grimme of DFT-D2 is used to describe the van der Waals (*vdW*) interaction between the substrate and LiPSs [39,40]. The models of *MXenes* are constructed using 3 × 3 super cells. The size of the vacuum layer is set to 20 Å along the Z-axis to avoid layer-to-layer interaction. To ensure the accuracy of the calculation, 520 eV is selected as the cut-off energy of the plane wave base. The 6 × 6 × 1 k-point grid is used for structural optimization, and the 9 × 9 × 1 k-point grid is used for the calculation of the density of states. Meanwhile, the maximum values of the energy standard, force standard position and displacement standard for structural convergence are 2×10^{-5} eV/atom^{-1}, 0.05 eV/Å^{-1} and 0.002 Å, respectively. The electron transfer is calculated using the Hirshfeld population analysis method.

The adsorption energy (E_{ads}) between Li_2S_x species and *MXenes* is defined by the following formula:

$$E_{ads} = E_{species+MXene} - (E_{species} + E_{MXene}) \quad (1)$$

where $E_{species+MXene}$ represents the energy of the entire system after *MXenes* adsorb Li_2S_x species, while E_{MXene} and $E_{species}$ represent the energy of isolated *MXenes* and Li_2S_x species, respectively. By definition, the more negative the value, the stronger ability of *MXenes* to adsorb Li_2S_x species.

3. Results and Discussion

3.1. Structure and Adsorption Performance

First, the structures of Li_2S_x species are studied (Figure 2). S_8 presents a folded ring structure, and the shortest S-S bond length is 1.96 Å. The shortest S-Li bond lengths of soluble Li_2S_8, Li_2S_6, and Li_2S_4 are 2.39 Å, 2.41 Å, and 2.37 Å, respectively, and the shortest S-S bond lengths are 2.05 Å, 2.04 Å, and 2.08 Å, respectively. For insoluble Li_2S_2 and Li_2S, the shortest S-Li bond lengths are 2.24 Å and 2.11 Å, respectively. For insoluble Li_2S_2 and Li_2S, the shortest S-Li bond lengths are 2.24 Å and 2.11 Å. All molecules present a 3D structure, not a chain structure, which is consistent with previous work [41].

Secondly, we establish the model of Ti_2N (Figure S1). The lattice constant is a = b = 3.01 Å, and the Ti-N bond length is 2.07 Å. Based on Ti_2N, the model of Ti_2NS_2 is established (Figure 3). The fully relaxed Ti_2NS_2 presents the hexagonal structure. The lattice constant is a = b = 3.17 Å. The triangular carbon layer in the middle is sandwiched by two triangular titanium layers, while the outermost layer of S atoms is located directly above the lower layer of titanium. Compared with the original Ti_2N, the Ti–N bond length of Ti_2NS_2 changes from 2.07 Å to 2.18 Å. The bond length of the Ti–S bond is 2.39 Å. This is in line with the results of previous research [42], indicating the correctness of the Ti_2NS_2 model.

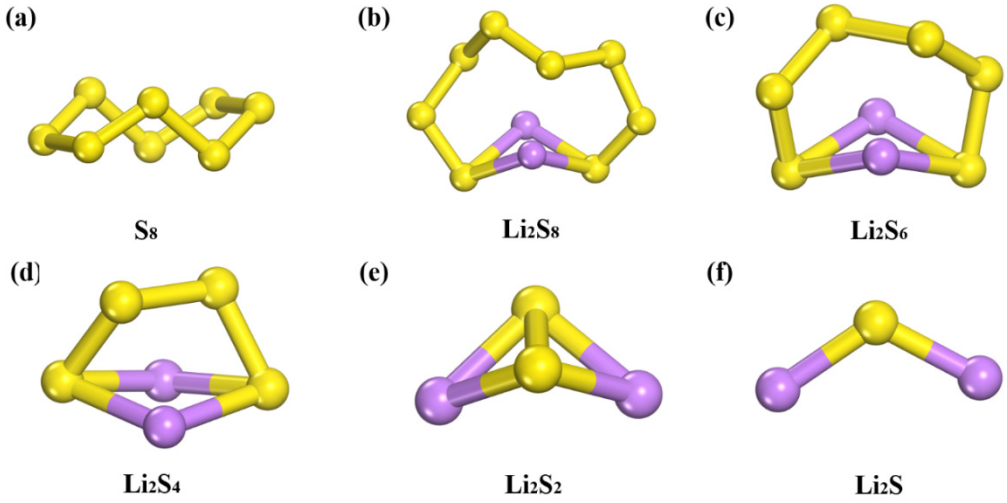

Figure 2. The structures of (**a**) S_8, (**b**) Li_2S_8, (**c**) Li_2S_6, (**d**) Li_2S_4, (**e**) Li_2S_2 and (**f**) Li_2S. Purple balls represent Li atoms. Yellow balls represent S atoms.

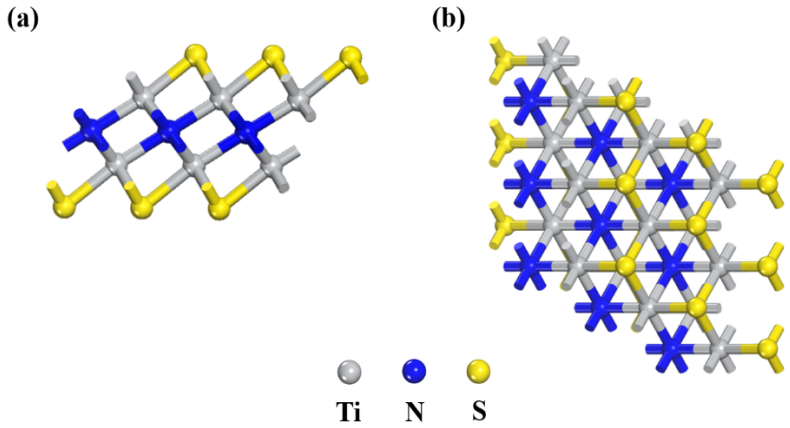

Figure 3. (**a**) Side and (**b**) top views of Ti_2NS_2. Yellow balls represent S atoms. Gray balls represent Ti atoms. Blue balls represent N atoms.

Figure 4 shows the density of states of Ti_2NS_2. The dotted line represents the Fermi energy levels. It can be clearly seen from the figure that the Fermi level appears in the electronic state, which indicates that the Ti_2N with S-functional group presents the metallicity. The metallicity is mainly provided by the d-orbital of titanium. At the same time, the p-orbital of the sulfur atom also contributes to the metallicity of Ti_2NS_2. The electrical conductivity of the host materials facilitates the charge-discharge reaction in Li-S batteries, since it can provide the electrons needed for the reaction.

After understanding the structure of Li_2S_x species and Ti_2NS_2, the interaction between Li_2S_x species and Ti_2NS_2 is studied. To find the stable structures, different positions of the Li_2S_x species on Ti_2NS_2 are tried. For Li_2S, the possible adsorption orientations include S-Top, Li-Side and S-Down (Figure S2). Among the three adsorption orientations, the S-Down becomes the S-Top after optimization, and the adsorption energies of the S-Top and Li-Side are −3.42 eV and −1.56 eV, respectively. Therefore, the S-Top is the most favorable adsorption orientation. The adsorption of Li_2S_2, Li_2S_4, Li_2S_6, Li_2S_8 and S_8 on Ti_2NS_2 is considered in a similar manner. The final optimized structures are shown in Figure 5. Table 1 shows the adsorption energies (E_{ads}), shortest distances between Li_2S_x species and Ti_2NS_2 (d), and transfer charge (Q) when Ti_2NS_2 adsorbs Li_2S_x species. The ring structure of the S_8 molecule remains intact, parallel to the surface of Ti_2NS_2, and the adsorption energy is −0.57 eV. The shortest distance between the S atom of S_8 and the S atom on the surface of Ti_2NS_2 is 3.52 Å. For insoluble Li_2S and Li_2S_2, their Li atoms tend to combine

with the S atoms of Ti_2NS_2. Li atoms of Li_2S and Li_2S_2 are surrounded by three S atoms on the surface of Ti_2NS_2, and the distances from the nearest S atoms are 2.38 Å and 2.43 Å, respectively, and the adsorption energies are −3.42 eV and −2.36 eV, respectively. As for the soluble Li_2S_4, Li_2S_6, Li_2S_8, their adsorption energies are −1.31 eV, −0.90eV, −0.95 eV, respectively. Similar to the insoluble Li_2S and Li_2S_2, Li atoms tend to combine with the S atoms of the Ti_2NS_2, and the shortest distances between them are 2.47 Å, 2.54 Å and 2.51 Å, respectively. Generally speaking, the adsorption energies of Ti_2NS_2 for Li_2S_x are between −0.57 eV~−3.42 eV, showing an increasing trend with the deepening of lithiation.

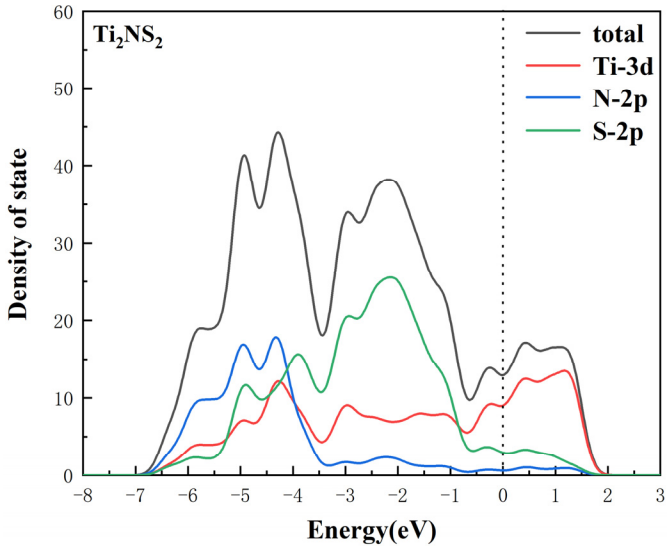

Figure 4. Density of states of Ti_2NS_2 (the dotted line indicates the Fermi energy level).

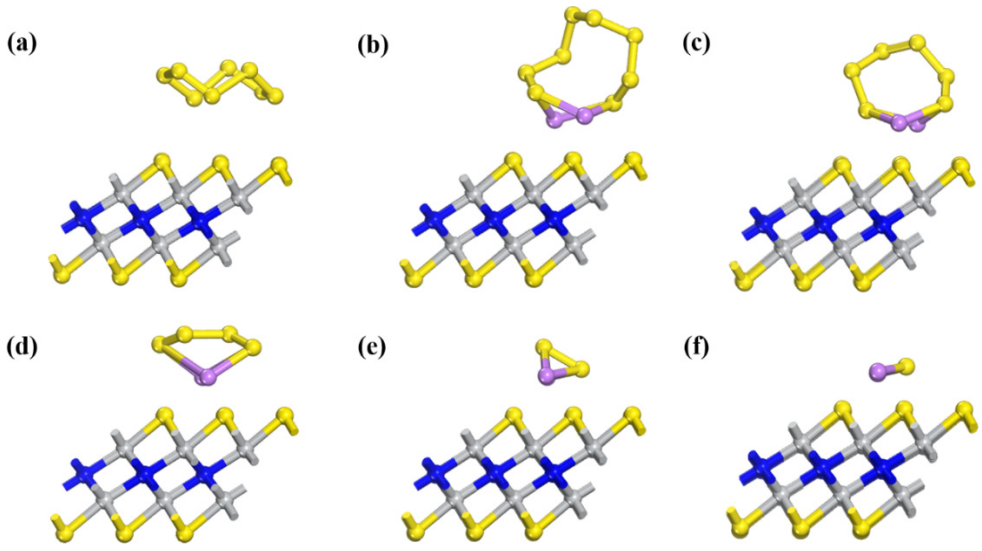

Figure 5. The optimized structures of Ti_2NS_2 absorbing (**a**) S_8, (**b**) Li_2S_8, (**c**) Li_2S_6, (**d**) Li_2S_4, (**e**) Li_2S_2, and (**f**) Li_2S. Purple balls represent Li atoms. Yellow balls represent S atoms. Gray balls represent Ti atoms. Blue balls represent N atoms.

Table 1. The adsorption energy (E_{ads}), shortest distance between Li_2S_x species and Ti_2NS_2, the charge transfer (Q, a positive value means that the substrate loses electrons from Li_2S_x, a negative value is the opposite) when Ti_2NS_2 adsorbs Li_2S_x species.

	Li_2S	Li_2S_2	Li_2S_4	Li_2S_6	Li_2S_8	S_8
E_{ads}/eV	−3.42	−2.36	−1.31	−0.90	−0.95	−0.57
d/Å	2.38	2.43	2.47	2.54	2.51	3.52
Q/e	0.38	0.34	0.22	0.13	0.15	0.13

Since the shuttle effect is caused by the dissolution of soluble polysulfides (Li_2S_4, Li_2S_6, and Li_2S_8) into the electrolyte, we calculate the adsorption energies of electrolyte solvent molecules (DOL and DME) for Li_2S_4, Li_2S_6, and Li_2S_8 (Figure S3). The results show that the adsorption energies of electrolyte solvent molecules are between −0.76~−0.84 eV, which are fewer than those of Ti_2NS_2 (−0.90~−1.31 eV). Furthermore, the adsorption energies of Ti_2NS_2 are in the range of −0.8~−2.0 eV [43], and the adsorption energy intensity is moderate. Therefore, Ti_2NS_2 can effectively inhibit the shuttle effect. In addition, to form a comparison, the model of Ti_2NO_2 is constructed (Figure S4). The structure of Ti_2NO_2 is similar to that of Ti_2NS_2, presenting a hexagon structure. The lattice constant of Ti_2NO_2 is a = b = 3.07 Å, and the length of the Ti–O bond is 1.85 Å, which is shorter than that of Ti_2NS_2, mainly because the size of the oxygen atom is smaller than that of the sulfur atom. After that, the adsorption energies of Ti_2NO_2 for Li_2S_x species are calculated (Figure S5, Figure 6). The results show that the adsorption energies of Ti_2NO_2 for Li_2S_x species are −2.07 eV, −2.21 eV, −1.29 eV, −0.66 eV, −0.90 eV, −0.43 eV, respectively, which are fewer than those of Ti_2NS_2. Therefore, Ti_2NO_2 is less effective than Ti_2NS_2 in inhibiting the shuttle effect. The S-functional groups have an advantage over the O-functional groups.

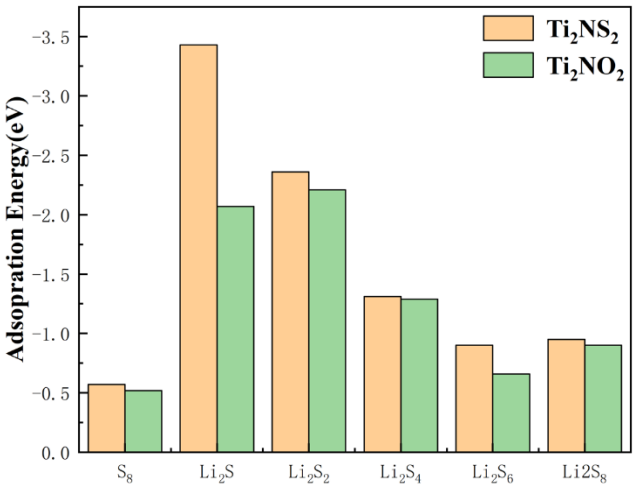

Figure 6. Adsorption energies of Ti_2NS_2 and Ti_2NO_2.

To further explore the adsorption mechanism of Ti_2NS_2, the charge transfer and charge density difference between Li_2S_x species and Ti_2NS_2 are calculated.

It can be seen from Table 1 that the transferred electrons between S_8 and Ti_2NS_2 are 0.13 e, which indicates that the force between S_8 and the substrate is weak, and the adsorption energy depends on van der Waals force. Similar to S_8, the transferred electrons of Li_2S_8 and Li_2S_6 are 0.15 e and 0.13 e, respectively, so the adsorption energies also mainly depend on van der Waals force. Later, with the deepening of lithium, the transferred electrons become more. The transferred electrons of Li_2S_4, Li_2S_2 and Li_2S are 0.22 e, 0.34 e and 0.38 e, respectively. Meanwhile, the adsorption energies become higher, indicating that the transferred electrons affect the adsorption energies.

Figure 7 shows the charge density difference between Li_2S_x species and Ti_2NS_2. The blue regions indicate the accumulation of charge, and the red regions indicate the depletion

of charge. The blue regions are mainly concentrated near the Li atoms of Li_2S_x and the S atoms of Ti_2NS_2 surface, which indicates that the transferred electrons between Li_2S_x species and Ti_2NS_2 surface are mainly provided by Li atoms of Li_2S_x species. For long-chain sulfides (Li_2S_8, Li_2S_6, Li_2S_4), the blue regions are significantly smaller than those of short-chain sulfides (Li_2S_2, Li_2S), indicating that the transferred electrons of long-chain sulfides are fewer than those of short-chain sulfides, so Ti_2NS_2 has a stronger adsorption capacity for short-chain sulfides.

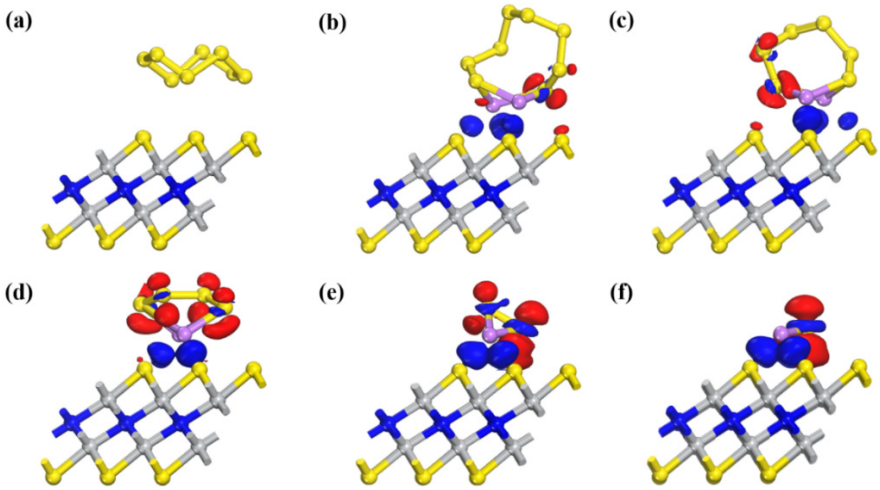

Figure 7. Charge density difference between (**a**) S_8, (**b**) Li_2S_8, (**c**) Li_2S_6, (**d**) Li_2S_4, (**e**) Li_2S_2, (**f**) Li_2S and Ti_2NS_2. The isosurface level is set to 0.025 e/Å^3. The blue regions indicate charge accumulation, and the red regions indicate charge depletion.

In addition, to better explore the influence of van der Waals forces on adsorption, we take Li_2S_2, Li_2S_4 and Li_2S_6 as examples to calculate the ratio of *vdW* interaction (*R*), as shown in Figure 8. The R is defined as follows:

$$R = \frac{E_{ads}^{vdW} - E_{ads}^{novdW}}{E_{ads}^{vdW}} \times 100\% \quad (2)$$

where E_{ads}^{vdW} and E_{ads}^{novdW} represent the adsorption energies with and without the *vdW* interaction, respectively. It is clear that the ratio of van der Waals forces decreases and the ratio of chemical interactions increases as the degree of lithium increases. For long-chain sulfides, van der Waals force is the main source of adsorption energy.

3.2. Electronic Properties

It is well known that good conductivity is very important for batteries. However, sulfur, the cathode material of Li-S batteries, is very poor in conductivity. An excellent cathode host material should not only have good conductivity itself, but also have good conductivity after absorbing Li_2S_x species. Therefore, the density of states of the whole systems after Ti_2NS_2 adsorbed Li_2S_x species is calculated. Figure 9a shows the density of states of the whole system after Ti_2NS_2 adsorbed S_8, and the dotted line in Figure 9 represents the Fermi energy level. Similar to the density of states of Ti_2NS_2, S_8@Ti_2Ns_2 composites still possess metallic properties due to Ti atoms. The electronic properties of S_8 are changed by Ti_2NS_2. In addition, Figure 9b–f show the density of states of the systems which are formed after the adsorption of long-chain sulfides Li_2S_8, Li_2S_6, Li_2S_4 and short-chain sulfides Li_2S_2 and Li_2S by Ti_2NS_2. Affected by Ti_2NS_2, the composite materials formed by Li_2S_x species and Ti_2NS_2 still have an electronic state at the Fermi level. All systems exhibit metallic properties, including S_8, Li_2S, and Li_2S_2, which are originally poor conductivities. This indicates that the sulfur cathodes can maintain high conductivity

during the entire lithiation and delithiation process. This is very beneficial for improving the cycle performance and rate performance of Li-S batteries.

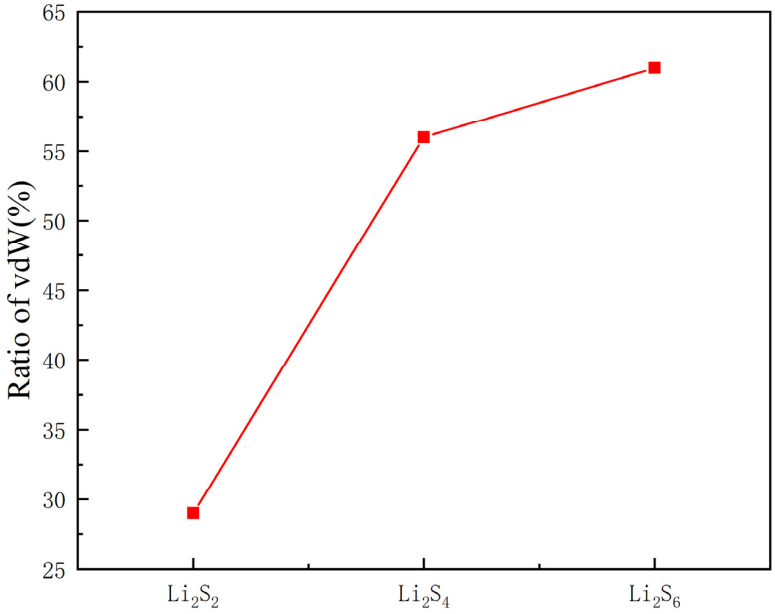

Figure 8. Ratios of *vdW* interaction for Li_2S_x (x = 2, 4, 6) species on Ti_2NS_2.

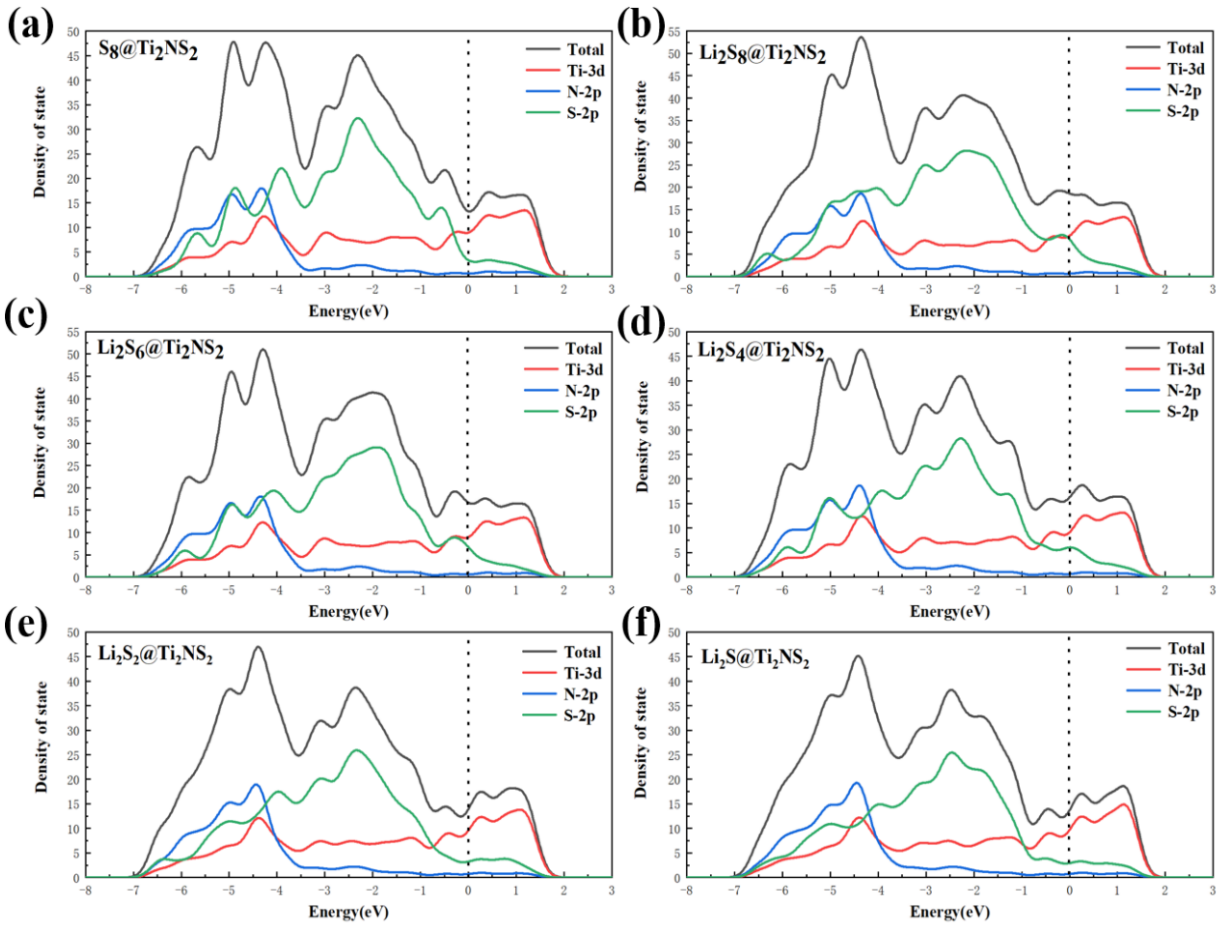

Figure 9. Density of states of (**a**) S_8, (**b**) Li_2S_8, (**c**) Li_2S_6, (**d**) Li_2S_4, (**e**) Li_2S_2 and (**f**) Li_2S anchored on Ti_2NS_2 (The dotted line indicates the Fermi energy level).

4. Conclusions

In this work, the performance of S-functionalized Ti_2N (Ti_2NS_2) as the host materials for the cathodes of Li-S batteries is studied through first-principles calculations. The results show that the adsorption energies of Ti_2NS_2 are moderate, stronger than those of Ti_2NO_2, especially the adsorption energies of LiPSs are stronger than those of electrolytes, which can effectively inhibit the shuttle effect. At the same time, Ti_2NS_2 has good conductivity without adsorption of Li_2S_x species. After adsorption of Li_2S_x species, it still has a high conductivity, which can improve the conductivity of sulfur cathodes and enhance the electrochemical activity during the charge/discharge process. Therefore, Ti_2NS_2 has the potential to be the cathode host materials for Li-S batteries. This work provides a reference for the design of high-performance cathode host materials.

Supplementary Materials: The following are available online at https://www.mdpi.com/article/10.3390/nano11102478/s1. Figure S1: (a) Side and (b) top views of Ti_2N. Gray balls represent Ti atoms. Blue balls represent N atoms. Figure S2: The possible orientation of Li2S with respect toTi_2NS_2. Figure S3: The optimized structures of DME and DOL absorbing (a) S_8, (b) Li_2S_8, (c) Li_2S_6, (d) Li_2S_4, (e) Li_2S_2, and (f) Li_2S. Figure S4: (a) Side and (b) top views of Ti_2NS_2. Red balls represent O atoms. Gray balls represent Ti atoms. Blue balls represent N atoms. Figure S5: The optimized structures of Ti_2NO_2 absorbing (a) S_8, (b) Li_2S_8, (c) Li_2S_6, (d) Li_2S_4, (e) Li_2S_2, and (f) Li_2S. Purple balls represent Li atoms. Red balls represent O atoms. Gray balls represent Ti atoms. Blue balls represent N atoms.

Author Contributions: C.Y.: Writing—review and editing. W.L.: Writing—original draft, Supervision, Project administration, writing review and editing. K.D.: Writing—review and editing. C.Z.: Writing—review and editing. J.L.: Writing—review and editing. Q.R.: Writing—original draft, G.B.: Writing—review and editing. All authors have read and agreed to the published version of the manuscript.

Funding: This work was supported by Natural Science Research Projects of Jiangsu Province University (20KJA510001), China Postdoctoral Science Foundation (2018T110480), Open Foundation of State Key Laboratory of Luminescent Materials and Devices (2020-skllmd-03), Open Research Fund of State Key Laboratory of Bioelectronics, Southeast University, Research Center of Optical Communications Engineering & Technology, Jiangsu Province (ZXF201904), and Postgraduate Research and Practice Innovation Program of Jiangsu Province (SJCX20_0249).

Conflicts of Interest: The authors declare that they have no known competing financial interests or personal relationships that could have appeared to influence the work reported in this paper.

References

1. Hameer, S.; Niekerk, J.L.V. A review of large-scale electrical energy storage. *Int. J. Energy Res.* **2015**, *39*, 1179–1195. [CrossRef]
2. Etacheri, V.; Marom, R.; Elazari, R.; Salitra, G.; Aurbach, D. Challenges in the development of advanced Li-ion batteries: A review. *Energy Environ. Sci.* **2011**, *4*, 3243–3262. [CrossRef]
3. Seh, Z.W.; Sun, Y.M.; Zhang, Q.F.; Cui, Y. Designing high-energy lithium-sulfur batteries. *Chem. Soc. Rev.* **2016**, *45*, 5605–5634. [CrossRef] [PubMed]
4. Liang, J.; Sun, Z.H.; Li, F.; Cheng, H.M. Carbon Materials for Li-S Batteries: Functional Evolution and Performance Improvement. *Energy Storage Mater.* **2016**, *2*, 76–106. [CrossRef]
5. Yin, Y.X.; Xin, S.; Guo, Y.G.; Wan, L.J. Lithium-Sulfur Batteries: Electrochemistry, Materials, and Prospects. *Angew. Chem.* **2013**, *52*, 13186–13200. [CrossRef]
6. Kang, W.M.; Deng, N.P.; Ju, J.G.; Li, Q.X.; Wu, D.Y.; Ma, X.M.; Li, L.; Naebe, M.; Cheng, B.W. A review of recent developments in rechargeable lithium-sulfur batteries. *Nanoscale* **2016**, *8*, 16541–16588. [CrossRef] [PubMed]
7. Wong, H.L.; Ou, X.W.; Zhuang, M.H.; Liu, Z.J.; Hossain, M.D.; Cai, Y.T.; Liu, H.W.; Lee, H.B.; Wang, C.Z.; Luo, Z.T. Selenium Edge as a Selective Anchoring Site for Lithium-Sulfur Batteries with $MoSe_2$/Graphene-Based Cathodes. *ACS Appl. Mater. Int.* **2019**, *11*, 19986–19993. [CrossRef]
8. Yang, Y.; Zheng, G.Y.; Cui, Y. Nanostructured sulfur cathodes. *Chem. Soc. Rev.* **2013**, *42*, 3018–3032. [CrossRef]
9. Li, T.; Cheng, H.; Zhang, W. A novel porous C_4N_4 monolayer as a potential anchoring material for lithium-sulfur battery design. *J. Mater. Chem. A* **2019**, *7*, 4134–4144. [CrossRef]
10. Chen, X.; Hou, T.Z.; Persson, K.A.; Zhang, Q. Combining theory and experiment in lithium–sulfur batteries: Current progress and future perspectives. *Mater. Today* **2019**, *22*, 142–158. [CrossRef]
11. Pang, Q.; Liang, X.; Kwok, C.Y.; Nazar, L.F. Advances in lithium-sulfur batteries based on multifunctional cathodes and electrolytes. *Nat. Energy* **2016**, *1*, 16132. [CrossRef]

12. Li, C.X.; Xi, Z.C.; Guo, D.X.; Chen, X.J.; Yin, L.W. Chemical Immobilization Effect on Lithium Polysulfides for Lithium-Sulfur Batteries. *Small* **2017**, *14*, 1701986. [CrossRef] [PubMed]
13. Hla, B.; Shuai, M.; Hca, B.; Hza, B. Ultra-thin Fe_3C nanosheets promote the adsorption and conversion of polysulfides in lithium-sulfur batteries-ScienceDirect. *Energy Storage Mater.* **2019**, *18*, 338–348.
14. Klein, M.J.; Veith, G.M.; Manthiram, A. Rational Design of Lithium-Sulfur Battery Cathodes Based on Experimentally Determined Maximum Active Material Thickness. *J. Am. Chem. Soc.* **2017**, *139*, 9229–9237. [CrossRef] [PubMed]
15. Li, S.H.; Leng, D.; Li, W.Y.; Qie, L.; Dong, Z.H.; Cheng, Z.Q.; Fan, Z.Y. Recent Progress in Developing Li2S Cathodes for Li-S. Batteries. *Energy Storage Mater.* **2020**, *27*, 279–296. [CrossRef]
16. Li, Z.; Wu, H.B.; Lou, X.W. Rational design and engineering of hollow micro-/nanostructures as sulfur hosts for advanced lithium-sulfur batteries. *Energy Environ. Sci.* **2016**, *9*, 3061–3070. [CrossRef]
17. Li, S.H.; Fan, Z.Y. Encapsulation methods of sulfur particles for lithium-sulfur batteries: A review. *Energy Storage Mater.* **2021**, *34*, 107–127. [CrossRef]
18. Ji, X.L.; Lee, K.T.; Nazar, L.F. A highly ordered nanostructured carbon-sulphur cathode for lithium-sulphur batteries. *Nat. Mater.* **2009**, *8*, 500–506. [CrossRef] [PubMed]
19. Ma, S.B.; Wang, L.G.; Wang, Y.; Zuo, P.J.; He, M.X.; Zhang, H.; Ma, L.; Wu, T.P.; Yin, G.P. Palladium nanocrystals-imbedded mesoporous hollow carbon spheres with enhanced electrochemical kinetics for high performance lithium sulfur batteries. *Carbon* **2019**, *143*, 878–889. [CrossRef]
20. Zhang, L.; Wu, B.; Li, Q.F.; Li, J.F. Molecular engineering lithium sulfur battery cathode based on small organic molecules: An ab-initio investigation. *Appl. Surf. Sci.* **2019**, *484*, 1184–1190. [CrossRef]
21. Wang, X.; Zhang, Z.; Qu, Y.H.; Lai, Y.Q.; Li, J. Nitrogen-doped graphene/sulfur composite as cathode material forhigh capacity lithium-sulfur batteries. *J. Power Sources* **2014**, *256*, 361–368. [CrossRef]
22. Hong, X.J.; Tang, X.Y.; Wei, Q.; Song, C.L.; Wang, S.Y.; Dong, R.F.; Cai, Y.P.; Si, L.P. Efficient Encapsulation of Small S_{2-4} Molecules in MOF-Derived Flowerlike Nitrogen-Doped Microporous Carbon Nanosheets for High-Performance Li-S. Batteries. *ACS Appl. Mater. Inter.* **2018**, *10*, 9435–9443. [CrossRef]
23. Ji, L.W.; Rao, M.M.; Zheng, H.M.; Zhang, L.; Li, Y.C.; Duan, W.H.; Guo, J.H.; Cairns, E.J.; Zhang, Y.G. Graphene Oxide as a Sulfur Immobilizer in High Performance Lithium/Sulfur Cells. *J. Am. Chem. Soc.* **2017**, *133*, 18522–18525. [CrossRef]
24. Zhang, Q.; Zhang, X.F.; Li, M.; Liu, J.Q.; Wu, Y.C. Sulfur-deficient MoS_{2-x} promoted lithium polysulfides conversion in lithium-sulfur battery: A first-principles study. *Appl. Surf. Sci.* **2019**, *487*, 452–463. [CrossRef]
25. Yan, L.J.; Luo, N.N.; Kong, W.B.; Luo, S.; Wu, H.C.; Jiang, K.L.; Li, Q.Q.; Fan, S.S.; Duan, W.H.; Wang, J.P. Enhanced performance of lithium-sulfur batteries with an ultrathin and lightweight MoS_2/carbon nanotube interlayer. *J. Power Sources* **2018**, *389*, 169–177. [CrossRef]
26. Yu, M.P.; Ma, J.S.; Song, H.Q.; Wang, A.J.; Tian, F.Y.; Wang, Y.S.; Qiu, H.; Wang, R.M. Atomic layer deposited TiO_2 on nitrogen-doped graphene/sulfur electrode for high performance lithium-sulfur battery. *Energy Environ. Sci.* **2016**, *9*, 1495–1503. [CrossRef]
27. Sun, J.; Sun, Y.M.; Pasta, M.; Zhou, G.M.; Li, Y.Z.; Liu, W.; Xiong, F.; Cui, Y. Entrapment of Polysulfides by a Black-Phosphorus-Modified Separator for Lithium-Sulfur Batteries. *Adv. Mater.* **2016**, *28*, 9797–9803. [CrossRef] [PubMed]
28. Wu, S.; Hui, K.S.; Hui, K.N. 2D Black Phosphorus: From Preparation to Applications for Electrochemical Energy Storage. *Adv. Sci.* **2018**, *5*, 1700491. [CrossRef] [PubMed]
29. Lu, L.; Chen, L.; Mukherjee, S.; Gao, J.; Sun, H.; Liu, Z.B.; Ma, X.L.; Gupta, T.; Singh, C.V.; Ren, W.C.; et al. Phosphorene as a Polysulfide Immobilizer and Catalyst in High-Performance Lithium-Sulfur Batteries. *Adv. Mater.* **2016**, *29*, 1602734.
30. Karlsson, L.H.; Birch, J.; Halim, J.; Barsoum, M.W.; Persson, P.O.A. Atomically Resolved Structural and Chemical Investigation of Single MXene Sheets. *Nano Lett.* **2015**, *15*, 4955–4960. [CrossRef]
31. Zhao, J.; Li, W.; Feng, Y.; Li, J.; Bai, G.; Xu, J. Sensing mechanism of hydrogen storage on Li, Na and K-decorated Ti_2C. *Appl. Phys. A* **2020**, *126*, 945. [CrossRef]
32. Xie, X.Q.; Zhao, M.Q.; Anasori, B.; Maleski, K.; Ren, C.E.; Li, J.W.; Byles, B.W.; Pomerantseva, E.; Wang, G.X.; Gogotsi, Y. Porous heterostructured MXene/carbon nanotube composite paper with high volumetric capacity for sodium-based energy storage devices. *Nano Energy* **2016**, *26*, 513–523. [CrossRef]
33. Liang, X.; Garsuch, A.; Nazar, L.F. Sulfur Cathodes Based on Conductive MXene Nanosheets for High-Performance Lithiu-Sulfur Batteries. *Angew. Chem.* **2015**, *54*, 3907–3911. [CrossRef] [PubMed]
34. Du, C.; Wu, J.; Yang, P.; Li, S.Y.; Xu, J.M.; Song, K.X. Embedding S@TiO_2 nanospheres into MXene layers as high rate cyclability cathodes for lithium-sulfur batteries. *Electrochim. Acta* **2018**, *295*, 1067–1074. [CrossRef]
35. Borysiuk, V.N.; Mochalin, V.N.; Gogotsi, Y. Molecular dynamic study of the mechanical properties of two-dimensional titanium carbides $Ti_{n+1}C_n$ (MXenes). *Nanotechnology* **2015**, *26*, 265705. [CrossRef]
36. Jimmy, J.; Kandasubramanian, B. MXene Functionalized Polymer Composites: Synthesis and Applications. *Eur. Polym. J.* **2019**, *122*, 109367. [CrossRef]
37. Wang, D.S.; Li, F.; Lian, R.Q.; Xu, J.; Kan, D.X.; Liu, Y.H.; Chen, G.; Gogotsi, Y.; Wei, Y.J. A General Atomic Surface Modification Strategy for Improving Anchoring and Electrocatalysis Behavior of $Ti_3C_2T_2$ MXene in Lithium-Sulfur Batteries. *ACS Nano* **2019**, *13*, 11078–11086. [CrossRef]
38. Perdew, J.P.; Ernzerhof, M.; Burke, K. Rationale for mixing exact exchange with density functional approximations. *J. Chem. Phys.* **1996**, *105*, 9982–9985. [CrossRef]

39. Zhao, Y.; Zhao, J. Functional group-dependent anchoring effect of titanium carbide-based MXenes for lithium-sulfur batteries: A computational study. *Appl. Surf. Sci.* **2017**, *412*, 591–598. [CrossRef]
40. Zhang, Q.; Zhang, X.F.; Xiao, Y.H.; Li, C.; Tan, H.H.; Liu, J.Q.; Wu, Y.C. Theoretical Insights into the Favorable Functionalized Ti_2C-Based MXenes for Lithium-Sulfur Batteries. *ACS Omega* **2020**, *5*, 29272–29283. [CrossRef]
41. Yin, L.C.; Liang, J.; Zhou, G.M.; Li, F.; Saito, R.; Cheng, H.M. Understanding the interactions between lithium polysulfides and N-doped graphene using density functional theory calculations. *Nano Energy* **2016**, *25*, 203–210. [CrossRef]
42. Shukla, V.; Jena, N.K.; Naqvi, S.R.; Luo, W.; Ahuja, R. Modelling High-performing Batteries with Mxenes: The case of S-functionalized two-Dimensional Nitride Mxene Electrode. *Nano Energy* **2019**, *58*, 877–885. [CrossRef]
43. Song, J.J.; Su, D.W.; Xie, X.Q.; Guo, X.; Bao, W.Z.; Shao, G.J.; Wang, G.X. Immobilizing Polysulfides with MXene-Functionalized Separators for Stable Lithium-Sulfur Batteries. *ACS Appl. Mater. Interfaces* **2016**, *8*, 29427–29433. [CrossRef] [PubMed]